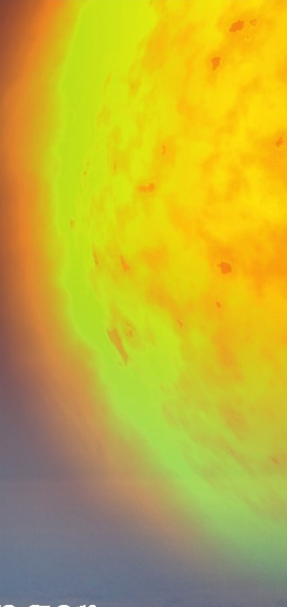
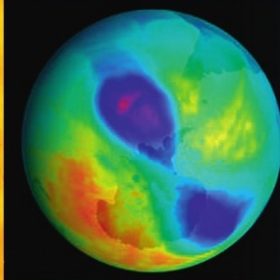
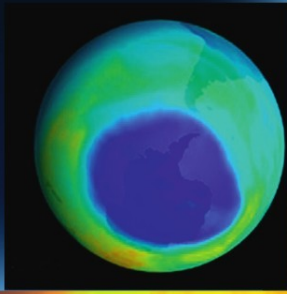


REMOTE SENSING AND ATMOSPHERIC OZONE

**Human Activities
versus Natural
Variability**



Arthur P. Cracknell
Costas A. Varotsos

 Springer

 PRAXIS

Remote Sensing and Atmospheric Ozone

Human Activities versus Natural Variability

Arthur P. Cracknell and Costas A. Varotsos

Remote Sensing and Atmospheric Ozone

Human Activities versus Natural Variability

 Springer

Published in association with
Praxis Publishing
Chichester, UK

PRAXIS

Professor Arthur P. Cracknell
Department of Applied Physics and
Electronic Engineering
University of Dundee
Dundee
U.K.

Professor Costas A. Varotsos
Faculty of Physics
Department of Environmental
Physics and Meteorology
University of Athens
Athens
Greece

SPRINGER-PRAXIS BOOKS IN ENVIRONMENTAL SCIENCES
SUBJECT ADVISORY EDITOR: John Mason, M.B.E., B.Sc., M.Sc., Ph.D.

ISBN 978-3-642-10333-9 ISBN 978-3-642-10334-6 (eBook)
DOI 10.1007/978-3-642-10334-6
Springer Heidelberg New York Dordrecht London

Library of Congress Control Number: 2011937034

© Springer-Verlag Berlin Heidelberg 2012

This work is subject to copyright. All rights are reserved by the Publisher, whether the whole or part of the material is concerned, specifically the rights of translation, reprinting, reuse of illustrations, recitation, broadcasting, reproduction on microfilms or in any other physical way, and transmission or information storage and retrieval, electronic adaptation, computer software, or by similar or dissimilar methodology now known or hereafter developed. Exempted from this legal reservation are brief excerpts in connection with reviews or scholarly analysis or material supplied specifically for the purpose of being entered and executed on a computer system, for exclusive use by the purchaser of the work. Duplication of this publication or parts thereof is permitted only under the provisions of the Copyright Law of the Publisher's location, in its current version, and permission for use must always be obtained from Springer. Permissions for use may be obtained through RightsLink at the Copyright Clearance Center. Violations are liable to prosecution under the respective Copyright Law.

The use of general descriptive names, registered names, trademarks, service marks, etc. in this publication does not imply, even in the absence of a specific statement, that such names are exempt from the relevant protective laws and regulations and therefore free for general use.

While the advice and information in this book are believed to be true and accurate at the date of publication, neither the authors nor the editors nor the publisher can accept any legal responsibility for any errors or omissions that may be made. The publisher makes no warranty, express or implied, with respect to the material contained herein.

Cover design: Jim Wilkie

Project management: OPS Ltd., Gt. Yarmouth, Norfolk, U.K.

Printed on acid-free paper

Springer is part of Springer Science+Business Media (www.springer.com)

Contents

Preface	xi
List of figures	xv
List of tables	xxiii
List of abbreviations and acronyms	xxvii
1 The traditional measurement of ozone concentration in the atmosphere	1
1.1 Introduction	1
1.1.1 Observations of the total ozone column	4
1.2 Ground-based instrumentation for TOC observations	5
1.2.1 The Dobson ozone spectrophotometer	7
1.2.2 Intercomparison of Dobson spectrophotometers	10
1.2.3 Interference of SO ₂ and NO ₂ in Dobson TOC measurements	19
1.2.4 Influence of stray light on Dobson TOC measurements	24
1.3 Brewer Spectrophotometer	34
1.4 Filter ozonometers M-83/124/134	37
1.5 Secondary ground-based instrumentation for TOC observations	39
1.5.1 System for Analysis of Observation at Zenith (SAOZ)	42
1.5.2 MICROTOPS II (Total Ozone Portable Spectrometer)	42
1.5.3 High-Resolution Visible/Ultraviolet Absorption Spectroscopy	43
1.5.4 Fourier transform spectrometer (FTS)	43
1.5.5 System for the Monitoring of Stratospheric Compounds (SYMOCS)	46
1.5.6 Star Pointing Spectrometer (SPS)	46
1.5.7 MDR-23 (a Russian commercial device)	46

1.5.8	Scanning spectrometer (EVA)	47
1.5.9	Solar IR spectroradiometer	47
1.5.10	Ground-based UV radiometer (GUV)	47
1.5.11	Spectrometer–Ozonometer PION	48
1.5.12	SPectrometer for Atmospheric TRAcers Monitoring (SPATRAM)	48
1.6	Observations of ozone vertical profile (OVP)	50
1.6.1	Primary ground-based instrumentation for OVP observations.	50
1.6.2	Dobson Umkehr measurements and inversion	51
1.6.3	Brewer Umkehr measurements	54
1.6.4	Secondary ground-based instrumentation for OVP observations	55
1.6.5	Lidar	55
1.6.6	Microwave radiometry	56
1.6.7	Ground-based Millimeter wave Ozone Spectrometer (GROMOS)	57
1.6.8	Stratospheric Sounding by Infrared Heterodyne Spectroscopy (SIRHS)	57
1.6.9	Ground-based microwave radiometers	58
1.6.10	Ground-based infrared solar spectroscopy	59
1.6.11	Stratospheric Ozone Monitoring Radiometer (SOMORA)	59
1.7	Airborne instrumentation for OVP observations	61
1.7.1	Electrochemical ozonesondes	61
1.7.2	Optical ozonesondes	64
1.7.3	Other balloon instrumentation	67
1.7.4	Aircraft instrumentation	71
1.8	Surface ozone measurements	77
1.8.1	Chemiluminescence method	77
1.8.2	Electrochemical potassium iodide method	77
1.8.3	UV absorption method	77
2	Satellite systems for studies of atmospheric ozone	79
2.1	Satellite remote sounding of TOC	82
2.2	Direct absorption measuring instruments	83
2.2.1	TIROS Operational Vertical Sounder (TOVS); GOES	83
2.2.2	Laser Heterodyne Spectrometer (LHS)/Tunable Diode LHS (TDLHS)	85
2.2.3	OZON-MIR	86
2.3	Indirect absorption measuring instruments	86
2.3.1	Total Ozone Mapping Spectrometer (TOMS)	86
2.3.2	Ozone Monitoring Instrument (OMI)	90
2.3.3	Advanced Earth Observing Satellite (ADEOS I, II)	93
2.3.4	Solar Backscattered Ultraviolet Radiometer (SBUV)	93
2.3.5	Global Ozone Monitoring Experiment (GOME)	96

2.3.6	ESA ENVISAT, GOMOS	98
2.3.7	The Ozone Mapping and Profiler Suite (OMPS) and the NPOESS	99
2.3.8	Ozone Dynamics Ultraviolet Spectrometer (ODUS) . . .	101
2.3.9	Ozone Layer Monitoring Experiment (OLME)	101
2.3.10	Interferometric Monitor for Greenhouse Gases (IMG) .	101
2.3.11	Infrared Atmospheric Sounding Interferometer	102
2.4	Observed variability in total ozone column	102
2.4.1	Latitudinal variation of TOC	102
2.4.2	Longitudinal variation of TOC	106
2.5	Satellite instrumentation for OVP observations	106
2.5.1	Direct-absorption measuring instruments	107
2.5.2	Scattering-measuring instruments	116
2.5.3	Emission-measuring instruments	118
2.5.4	Summary of ozone-monitoring satellites	130
2.6	Observed variability in vertical ozone distribution	130
2.6.1	EASOE	141
2.6.2	SESAME	142
2.6.3	THESEO	142
2.6.4	SOLVE	142
2.6.5	ORACLE-O ₃	143
2.6.6	SCOUT-O3	144
2.6.7	Match	144
2.6.8	ARC_IONS	145
3	Intercomparisons between various atmospheric ozone datasets.	149
3.1	Introduction	149
3.2	Total ozone measurements over Athens: intercomparison between Dobson, TOMS (version 7), SBUV, and other satellite measure- ments	152
3.3	Geophysical validation of MIPAS-ENVISAT operational ozone data	161
3.3.1	Introduction to MIPAS	161
3.3.2	MIPAS ozone data	163
3.3.3	Comparison of MIPAS data with WMO/GAW ground- based measurements	164
3.4	Comparison of MIPAS data with stratospheric balloon and aircraft measurements	190
3.4.1	MIPAS-B2	190
3.4.2	FIRS-2 and IBEX	193
3.4.3	SPIRALE	198
3.4.4	MIPAS-STR, SAFIRE-A, and FOZAN on board the M-55 <i>Geophysica</i> aircraft	200
3.4.5	ASUR	207

3.5	Comparison with satellite measurements.	208
3.5.1	Comparison of MIPAS data with SAGE II O ₃ profiles	211
3.5.2	Comparison with POAM III O ₃ profiles	213
3.5.3	Comparison with Odin-SMR O ₃ profiles	216
3.5.4	Comparison with ACE-FTS O ₃ profiles.	220
3.5.5	Comparison with HALOE O ₃ profiles.	223
3.5.6	Comparison with GOME O ₃ profiles	229
3.5.7	Comparison with SCIAMACHY and GOMOS.	231
3.6	Comparison of MIPAS data with ECMWF assimilated fields.	234
3.7	Summary of MIPAS comparisons.	236
3.8	Other intercomparisons between various ozone-monitoring systems	244
3.8.1	TOMS, GOME, GOMOS, and SCIAMACHY data	245
3.8.2	MLS data	248
3.8.3	SAGE data	249
3.8.4	TES data	250
3.8.5	ACE and IASI data	250
3.8.6	Ozonesonde intercomparisons	254
4	The dynamics of atmospheric ozone	255
4.1	Total ozone trends	257
4.2	Ozone vertical profile variability.	273
4.3	General features of ozone global distribution	287
4.3.1	Stratosphere–troposphere exchange	293
4.3.2	Low-ozone pockets	298
4.4	The non-linear nature of ozone variability; detrended fluctuation analysis (DFA)	306
4.4.1	Long-memory processes in global ozone and temperature variations	307
4.4.2	Long-term memory dynamics of total ozone content	314
4.4.3	Scaling behavior of the global tropopause	317
4.4.4	Scaling properties of air pollution at the surface; surface ozone (SOZ)	321
4.5	Impacts of the solar eclipse of March 29, 2006 on surface ozone and related air pollutants	322
4.6	Long-term coupling between TOC and tropopause properties	327
4.6.1	Occurrence frequency of tropopause height	329
4.6.2	Association between tropopause properties and TOC	333
4.6.3	The tropopause; summary.	336
5	The Montreal Protocol	339
5.1	Introduction.	339
5.2	The proposition by Molina and Rowland of human releases of CFCs being responsible for ozone depletion	340
5.3	The science from 1974 to 1985.	344

5.4	The Ozone Hole	351
5.5	The role of remote sensing in the lead-up to the Montreal Protocol	358
5.6	The NOZE and AAOE expeditions	358
5.7	Theories of the Ozone Hole	363
5.8	Diplomacy, 1974–1989; formulation and ratification of the Montreal Protocol	366
5.9	Reasons for the success in reaching international agreement in Montreal	368
5.10	Ratification of the Montreal Protocol	372
6	The study of atmospheric ozone since 1987	379
6.1	Introduction	379
6.2	The reduction of ozone-destroying chemicals in the atmosphere	379
6.2.1	Ozone depletion potential (ODP)	382
6.2.2	Equivalent Effective Stratospheric Chlorine (EESC)	385
6.3	Ground-based and ozonesonde data on ozone depletion	388
6.4	Piecewise linear trends in ozone depletion	390
6.5	Recovery of the ozone layer; the polar regions	406
6.5.1	Sudden stratospheric warmings	415
6.5.2	Observation of sudden stratospheric warmings detected in deep underground muon data	417
6.5.3	The role of the diffusion of gases in ice or an amorphous binary mixture in the polar stratosphere and the upper troposphere	420
6.5.4	Experimental studies of the Antarctic ozone hole and ozone loss in the Arctic	425
6.5.5	Antarctic ozone hole predictability; use of natural time series	441
6.6	Long-term monitoring of the ozone layer	448
6.6.1	Measurement of TOC and the OVP	452
6.6.2	The use of models to predict ozone concentration	454
6.6.3	Ozonesonde networks	469
6.6.4	Trends in TOC and tropopause properties	474
6.7	Scientific assessment of ozone depletion 2010	478
7	Atmospheric ozone and climate	485
7.1	Introduction	485
7.2	Radiative-forcing calculations.	492
7.2.1	Estimates of changes in RF from pre-industrial times to the present.	492
7.2.2	Detailed studies of changes in RF in recent decades	497
7.2.3	Contribution of the transport sector	515
7.3	Ozone-induced climatic impacts	517
7.3.1	The health impacts of changes in ozone concentration	543

x Contents

7.4	Conclusions on tropo-stratospheric variability	544
7.4.1	Stratospheric ozone dynamics and its determining factors	545
7.4.2	Tropospheric processes	546
7.5	New climate research aspects deduced from global ozone dynamics research and remote sensing	547
7.5.1	Climate modeling and atmospheric ozone	547
7.5.2	Role of phase transitions in climate system dynamics. . .	549
7.5.3	Nambu dynamics and ozone–climate modeling	550
7.5.4	Dissipation-induced instabilities in ozone and climate fields	551
7.5.5	Deterministic, chaotic, or stochastic ozone–climate time series	553
7.6	WMO/UNEP Scientific Assessment 2010	554
	References and bibliography.	559
	Index	653

Preface

Ozone is so rare in the atmosphere (there are only about three ozone molecules per 10 million air molecules) that if it was brought down to the Earth's surface and compressed to standard temperature and pressure, it would form a layer about as thick as a small coin. In spite of this, the importance of ozone, particularly in protecting the biosphere from the harmful effects of solar ultraviolet radiation, vastly exceeds what one might expect from this minor trace gas in the atmosphere. In the mid 1970s some scientists alerted the world to the fact that atmospheric ozone (which is mostly in the stratosphere) was being destroyed by manufactured chemicals released into the atmosphere. This led in 1987 to the Montreal Protocol to protect the ozone layer, which has been ratified by virtually every country in the world.

Remote sensing, which is mostly concerned with using Earth-orbiting satellites to study the Earth, played a vital role in the events leading up to the Montreal Protocol and since then has continued to play an important role in monitoring the implementation of the Montreal Protocol. The era of satellite remote sensing began on October 4, 1957, when the former Soviet Union launched Sputnik 1, the world's first artificial satellite (a 55 cm diameter sphere that weighed 83 kg with four antennae attached to it). It circled the Earth once every 96 minutes and transmitted radio signals that could be received on Earth. On November 3, 1957, a second satellite, Sputnik 2, was launched carrying a dog named Laika. The United States launched its first satellite, Explorer 1, on January, 31 1958, and its second, Vanguard 1, on March 17, 1958.

The launch of Sputniks 1 and 2 over 50 years ago marked the beginning of a long period of successful launches of a large number of Earth-orbiting unmanned spacecraft for environmental observation. Earth-orbiting satellites now play a crucial role in studying resources and environmental conditions in the atmosphere, biosphere, cryosphere, geosphere, and the oceans; in particular, in the present context they are involved in studying atmospheric ozone. Traditional measurements of atmospheric ozone from the ground, using ultraviolet spectrophotometers, and

from ozonesonde balloons were being made for many years before remote-sensing satellites came to be developed and operated. However, these traditional methods only measured ozone concentrations at a few points on the surface of the Earth. The advantage of remote sensing is that it provides frequent coverage of the whole Earth.

This book is concerned with showing how remote sensing contributes to the study of atmospheric ozone and the consequences of human activities on atmospheric ozone. We cover the traditional measurement of ozone concentration in the atmosphere and give a comprehensive description of the large number of different satellite systems for the study of atmospheric ozone. This is followed by a consideration of the consistency of the ozone observations obtained with different methodologies and techniques and the importance of intercomparisons between various atmospheric ozone datasets and between various ozone-monitoring systems. We give a summary of the state of knowledge of the dynamics of atmospheric ozone and then consider the Montreal Protocol, how it came about and how its implementation is being monitored.

Remote sensing played a key role in the scientific research that led to the Montreal Protocol on ozone-depleting substances and it continues to play an important role in the monitoring of the success of the Protocol (we edited a special issue of the *International Journal of Remote Sensing* on Remote Sensing and the Implementation of the Montreal Protocol, Volume 30, Numbers 15–16, August 2009). Our introductory paper in that special issue (pp. 3853–3873) forms the basis of Chapter 5 of this book. In this context, the topic on the evolution of the Antarctic ozone hole is discussed based on the proposition by Mario Molina and Sherwood Rowland that human manufacture and release of CFCs (chlorofluorocarbons) into the atmosphere causes ozone depletion.

In view of various criticisms of the Intergovernmental Panel on Climate Change (IPCC) and a general feeling of depression induced by the apparent slowness of the international community in addressing the problems of global warming and climate change, it is perhaps instructive to consider the relation between the Montreal Protocol and the Kyoto Protocol and we do discuss this question.

We end with a summary of the results of research work since 1987 (i.e., since the Montreal Protocol was formulated). This involves the study of ozone depletion, both the steady decline in concentration amounting to a few percent per decade, depending on location, and the catastrophic temporary development of the ozone hole for a few months each year in the Antarctic and, more recently, in the Arctic. It also involves the relation between changes in ozone and climatic conditions.

In some ways this book is a sequel to *Atmospheric Ozone Variability: Implications for Climate Change, Human Health and Ecosystems*, by K.Ya. Kondratyev and C.A. Varotsos (Springer/Praxis, 2000). However, a great deal has happened since that book was written, both in terms of new remote-sensing systems and results and in connection with long-term datasets and ozone depletion. We now concentrate here on the science of studying atmospheric ozone itself, principally using remote-sensing techniques. In writing the present book, we have relied on many sources of information, including of course papers from research journals, the proceedings of the various Quadrennial Ozone Symposia and the Reports on the Scientific

Assessment of Ozone Depletion by WMO/UNEP (the World Meteorological Organization and the United Nations Environment Program), which we have listed in our Table 6.1. However, when it came to the 2008 Quadrennial Ozone Symposium held in Tromsø, Norway, no proceedings volume was published; only a set of abstracts was produced and it was left to participants to publish their work in refereed journals. We have made extensive use of these abstracts and they enabled us to find many recently published papers that we have cited, but we have not cited any of the Tromsø abstracts themselves.

We are grateful to many present and former students and colleagues who have contributed to our understanding of remote sensing and atmospheric ozone.

Inevitably, we have reproduced a large amount of copyright material and we are grateful to the various copyright holders who have given their permission and who are acknowledged *in situ* in the text, figures, or tables. Every effort has been made to trace original copyright holders of previously published material but with mergers in the publishing industry it is not always possible to track them down, so we offer our apologies where any have been overlooked. We are very grateful to Clive Horwood, of Praxis Publishing, for his help and encouragement during the writing of this book and to the staff of OPS for their production work.

Arthur P. Cracknell
Costas A. Varotsos
September 2011

Figures

1.1	Sputnik 1 (a basketball in diameter with mass 83 kg), and ENVISAT with various instruments on board	2
1.2	The vertical distribution of atmospheric ozone: partial pressure of ozone and height	2
1.3	TOC at Table Mountain, California, as a function of season from three different TOC datasets from the 1920s to 1940s	6
1.4	The O ₃ spectrum at room temperature	6
1.5	Prof. G.M.B. Dobson with his co-worker Dr. D. Walshaw around 1970, and Dobson spectrophotometer optical diagram	8
1.6	Photo from the Dobson Intercomparison held in Arosa (July–August 1990)	16
1.7	$\Delta N_i = (N_i \text{ for Dobson D065} - N_i \text{ for Dobson D118}), i = A, C, D$, on August 5, 1990, versus $\mu = \sec \theta$; and Dr. D. Walshaw with Dr. C. Varotsos around 1985	17
1.8	N_C/μ_C versus μ_C for both D065 and D118, and the same but for the pairs D and A, respectively	18
1.9	$\Delta N_i = (N_i \text{ for Dobson D064} - N_i \text{ for Dobson D118})$, where $i = A, C, D$ on July 11, 2006, versus μ	19
1.10	N_C/μ_C versus μ_C for both D064 and D118, and the same but for the pairs D and A, respectively	20
1.11	Mean daily percentage error in TOC caused by SO ₂ for December to March and May to August of the 2-year period 1989–1990	23
1.12	Mean daily percentage error in TOC caused by NO ₂ for December to March of the 2-year period 1989–1990	24
1.13	Illustration of the effect of stray light on log intensity ratios and on the determination of extraterrestrial constants	26
1.14	Variation of ozone error X_{AD} as a function of airmass, μ , for various values of model parameters, as calculated by the stray light model	29
1.15	Comparison of experimental data with stray light models	30
1.16	Variation of ozone error X_{AD} as a function of airmass μ for $R_0 = 10^{-4.0}$ as calculated by Basher’s stray light model	31
1.17	As Figure 1.16, but for $R_0 = 10^{-3.0}$	31

1.18	Comparison between experimental data and stray light model values for November 27, 1992 and December 7, 1992	33
1.19	Brewer Mark IV mechanical assembly (top view)	34
1.20	Map showing the location of total ozone stations where data were submitted to WMO within the period of 1979–2006.	38
1.21	Schematic diagram of M-124 Ozonometer	39
1.22	Differential absorption cross-sections of some trace gases absorbing in the UV/visible wavelength region	41
1.23	Optical diagram of a Michelson interferometer; in one of the arms the mirror can be moved to lengthen or shorten the optical path.	44
1.24	SPATRAM (SPectrometer for Atmospheric TRAcers Monitoring) installed since April 2004 at the University of Évora, Portugal.	49
1.25	The SOMORA instrument	60
1.26	A schematic diagram of the Japanese ozonesonde and of an electrochemical concentration cell ozonesonde	65
1.27	A schematic diagram of the Indian ozonesonde	66
1.28	The M55 <i>Geophysica</i> high-altitude aircraft.	72
1.29	Photograph of the GAMS spectrometer	76
1.30	Advanced Pollution Instruments (API) Model 400E Ultraviolet Absorption Ozone analyzer	78
2.1	A NASA Global Hawk lands at Dryden, and the A-Train	81
2.2	TOMS optical diagram and the Nimbus-7 spacecraft which carried the first TOMS instrument, before its launch in 1978	88
2.3	Schematics of GOME Optics	97
2.4	Monthly trends in total ozone in the Mediterranean region and at Athens compared with the trends derived from zonally averaged data.	105
2.5	A cross-section of monthly trends in column ozone over the latitude belt 35°N–45°N derived from the 13 years of Nimbus-7 TOMS measurements.	106
2.6	Trends of differences between ozone measurements made by various ozone-profiling instruments and SAGE-II.	109
2.7	HALOE instrument.	111
2.8	The ACE-FTS instrument	113
2.9	Photograph of the MAESTRO instrument, showing occultation (solar) and backscatter viewing ports.	114
2.10	HIRDLS components	123
2.11	The MetOp satellite carrying the IASI instrument	126
2.12	The scanning mirror of IASI directing emitted infrared radiation from one swath into the uncovered interferometer	127
2.13	Cloud detail view from an image taken in Aberdeen (Scotland) with a digital camera	140
2.14	Locations of IONS sites.	145
2.15	Comparisons of several Canadian air quality models with IONS-04 sondes at the surface to 4 km	146
3.1	Scatter diagram for TOMS (version 7) and Dobson observations at Athens, Greece (March 1, 1991–December 31, 1991). All days.	154
3.2	Scatter diagram for SBUV (version 7) and Dobson observations at Athens, Greece (March 1, 1991–December 31, 1991). All days.	154
3.3	Scatter diagram for TOMS (version 7) and Dobson observations at Athens, Greece (March 1, 1991–December 31, 1991). Cloud-free days	155

3.4	Scatter diagram for SBUV (version 7) and Dobson observations at Athens, Greece (March 1, 1991–December 31, 1991). Cloud-free days	155
3.5	Intercomparison of column ozone observations performed by satelliteborne and ground-based instrumentation in Athens, Greece (2002–2006)	158
3.6	Comparison of column ozone observations performed by satelliteborne and ground-based instrumentation in Athens, Greece during 2002–2008	159
3.7	Comparison of monthly mean column ozone observations performed by satelliteborne and ground-based instrumentation in Athens, Greece during 1991–2008.	159
3.8	Time series of the percentage relative difference in ozone partial column (75–35 hPa) between MIPAS and correlative ozonesonde data at five western and central European stations for 2003	171
3.9	Vertically resolved statistics of the absolute differences between MIPAS O ₃ data and NDACC and WOUDC measurements in the Arctic.	173
3.10	Vertically resolved statistics of the relative differences between MIPAS O ₃ data and NDACC and WOUDC measurements in the Arctic.	174
3.11	Results of the comparison between MIPAS O ₃ profiles and ground-based lidar measurements matching the coincidence criteria of 400 km and 10 h.	177
3.12	Results of the comparison between MIPAS O ₃ profiles and ground-based lidar measurements: zonal averages.	181
3.13	Time series of ozone partial columns.	184
3.14	Statistical means and standard deviations of the relative differences between MIPAS and FTIR O ₃ profiles	186
3.15	Results of statistical analysis for MIPAS O ₃ bias and precision determination by comparison with matching measurements from mid-latitude ozone soundings.	191
3.16	Results of the comparison between coincident MIPAS-ENVISAT and MIPAS-B2 ozone measurements at mid-latitudes and in the Arctic region	195
3.17	Absolute difference between MIPAS-ENVISAT and MIPAS-B2 ozone volume mixing ratios averaged over all the available collocations	196
3.18	Comparison between MIPAS v4.61 and FIRS-2 (October 30, 2002 and September 19/20, 2003) ozone measurements	197
3.19	Comparison between MIPAS v4.61 and IBEX (July 29–30, 2002) ozone measurements	198
3.20	Comparison of MIPAS O ₃ profiles from orbit 4,678, scan 6 with the <i>in situ</i> profiles acquired during the SPIRALE flight	199
3.21	Comparison of MIPAS O ₃ profiles for orbit 4,677, scan 20 with the <i>in situ</i> profiles acquired during the SPIRALE flight	201
3.22	Results of the comparison between MIPAS-ENVISAT v4.61 ozone data and correlative measurements performed by the remote-sensing and <i>in situ</i> payload of the M-55 <i>Geophysica</i> aircraft during mid-latitude flights on July 22, 2002 and on October 24, 2002 from Forlì, Italy	205
3.23	Results of the comparison between MIPAS-ENVISAT v4.61 ozone data and correlative measurements performed by the remote-sensing and <i>in situ</i> payload of the M-55 <i>Geophysica</i> aircraft during high-latitude flights on March 2, 2003 and March 12, 2003 from Kiruna, Sweden	206
3.24	False-color map of potential vorticity on the isentropic surface $\theta = 420$ K and the M-55 <i>Geophysica</i> route during the ENVISAT validation flight from Kiruna on March 12, 2003	207

3.25	The absolute and percentage difference between the MIPAS and ASUR ozone profiles in the tropics, mid-latitudes, the Arctic	209
3.26	Comparison between MIPAS and SAGE II: statistics over all the collocated O ₃ profiles	213
3.27	Comparison between MIPAS and SAGE II: zonal averages	214
3.28	Comparison between MIPAS and SAGE II: seasonal averages	215
3.29	Comparison between MIPAS and POAM III: statistics over all the collocated O ₃ profiles	217
3.30	Comparison between MIPAS and POAM III O ₃ profiles: zonal averages . . .	219
3.31	Comparison between MIPAS and POAM III: seasonal averages for the Northern Hemisphere (60°N–90°N) and Southern Hemisphere high latitudes	220
3.32	Comparison between MIPAS and Odin-SMR: statistics over all the collocated O ₃ profiles	222
3.33	Comparison between MIPAS and ACE-FTS: statistics over all the collocated O ₃ profiles	224
3.34	Comparison between MIPAS and HALOE: statistics over all the collocated O ₃ profiles	225
3.35	Comparison between MIPAS and HALOE O ₃ profiles: zonal averages	226
3.36	Comparison between MIPAS and HALOE O ₃ profiles: seasonal averages . .	227
3.37	Comparison between MIPAS and GOME O ₃ profiles.	231
3.38	Comparison between MIPAS and GOME O ₃ profiles: zonal averages	232
3.39	MIPAS v4.61 and ECMWF O ₃ VMR mean profiles: global averages and corresponding mean relative difference, standard deviation, and MIPAS errors	236
3.40	Comparison between MIPAS v4.61 and ECMWF O ₃ VMR mean profiles: zonal and seasonal averages	239
3.41	Summary plot of global mean relative differences between MIPAS O ₃ VMR profiles and coincidence measurements by concurrent satellite sensors	240
3.42	Bruker 125HR installed at Polar Environment Atmospheric Research Laboratory (PEARL), located on Ellesmere Island, Canada	251
3.43	Monthly average of the relative differences of collocated ozone column measurements of SBUV(/2) with lidar, SAGE II, and Umkehr at 15.8–10 hPa	253
3.44	Comparison of ozone measurement, relative to a standard ozone photometer instrument, as measured by different combinations of ECC instrument type (ENSCI or SPC) and sensing solution types in intercomparisons	253
4.1	SBUV(/2), Dobson, and TOMS seasonal total ozone trends in percent per decade by latitude to May 1991	266
4.2a	Time series of decadal mean total column ozone (1850–1859 to 2000–2009) .	269
4.2b	Decadal annual means for tropospheric column ozone	270
4.3	Average total ozone in polar regions.	271
4.4	Monthly distribution of the occurrence of each group of ozone soundings for the period from November 1996 to April 1997 over Athens, Greece.	276
4.5	Ozone partial pressure, relative humidity, and temperature over Athens on January 24, 1997 and November 23, 2004	277
4.6	Ozone partial pressure, relative humidity, and temperature over Athens on April 6, 1997 and June 1, 2005	278
4.7	Ozone partial pressure, relative humidity, and temperature over Athens on January 10, 1997 and April 18, 2005	279
4.8	Ozone partial pressure, relative humidity, and temperature over Athens on April 1, 1997 and February 18, 2005	280

4.9	Ozone partial pressure, relative humidity, and temperature over Athens on February 6, 1997 and March 15, 2005.	281
4.10	A series of BUV instruments have been measuring ozone vertical distribution since 1970; vertical distribution of Arctic and Antarctic ozone.	286
4.11	Vertical–latitudinal cross-sections of past values and long-term changes for annual mean vertical residual velocity and ozone using an ensemble mean of three simulations from the CMAM.	287
4.12	Latitude–time cross-sections of total ozone deviations from 1964 to 1980 “norms” in percent	289
4.13	Variation in total ozone with latitude and season for two time intervals: 1964–1980 and 1984–1993	290
4.14	Difference between total ozone values for the two periods (1964–1980 and 1984–1993) reported in Figure 4.12.	291
4.15	Barnes map of gridded output ozone from a Lagrangian chemical model. . .	300
4.16	Equivalent solar latitude along 14-day diabatic back trajectories for air parcels used in the chemistry–trajectory model on March 9, 1993 at the 850 K surface	301
4.17	TOC mean monthly values in Dobson units during 1964–2004, over the belt 25°S–25°N derived from the WMO Dobson Network.	310
4.18	Log-log plot of the TOC root-mean-square fluctuation function versus temporal interval for deseasonalized TOC values	311
4.19	Log-log plot of the TRT root-mean-square fluctuation function versus time interval for deseasonalized TRT values	313
4.20	Log-log plot of the RMS fluctuation function for the smoothed and detrended reconstructed TOC time series, versus time interval and the respective best fit equation and correlation coefficient at Arosa and Poluy River.	317
4.21	Log-log plot of tropopause height root-mean-square fluctuation function versus time interval for the detrended and deseasonalized monthly Z values observed by the radiosonde network over the equator and the globe during 1980–2004.	319
4.22	Map with the locations of the monitoring stations	324
4.23	Surface ozone measurements and the expected surface ozone values as derived from the fitted curve of measurements before, during, and after the eclipse event of March 29, 2006 at four stations	325
4.24	SUVR-B measurements derived from the MICROTOPS II sun-photometer before, during, and after the solar eclipse of March 29, 2006, at Athens. . . .	326
4.25	SUVR measurements derived from the VLX-3W radiometer before, during, and after the solar eclipse of March 29, 2006, at Athens.	327
4.26	Nitrogen dioxide measurements before, during, and after the solar eclipse of March 29, 2006 at four stations	328
4.27	Occurrence frequency for the first tropopause height classes at Athens during 1984–2002.	330
4.28	Seasonal variability of the first and second thermal tropopause over Athens, Greece	331
4.29	Relative frequency of occurrence of the second tropopause over Athens, Greece	332
4.30	Temperature trends of the first and second tropopause over Athens, Greece .	333
4.31	Relation between TOC and tropopause height for average TOC values of different tropopause height classes, as deduced from Athens observations. . .	334

4.32	Seasonal variability in ozone partial pressure in the troposphere and the lower stratosphere at Athens as deduced from ozonesonde ascents throughout the period 1991–2001	334
5.1	Schematic diagram of the CFC impact on the ozone layer	348
5.2	Differences in average ozone concentrations 1970–1988 versus 1931–1969. . .	350
5.3	Percentage change in ozone 1976–1986 versus 1965–1975, Northern Hemisphere Dobson stations	350
5.4	South Pole ozone profiles in 2006 before the ozone hole developed and for the sounding that displayed the minimum ozone	353
5.5	Total ozone over Halley Bay, Antarctica, in October (southern spring)	355
5.6	Schematic diagram of the role of NO ₂ in ozone depletion.	360
5.7	Schematic diagram of polar ozone destruction.	364
5.8	Production and consumption trends for CFCs.	376
5.9	Production and consumption trends for halons	377
6.1	Antarctic ozone in October (averaged poleward of 70°) for four different simulations from the NASA/GSFC coupled chemistry–climate model	386
6.2	Hockey stick statistical trend model in the style of Reinsel <i>et al.</i> (2002, 2005)	391
6.3	Monthly TOC over Athens, Greece, from 1979 to 1999	392
6.4	Trends calculated for SAGE I/II for 1979–1991	393
6.5	Latitude–altitude cross-section of stratospheric ozone trends from various data sources.	394
6.6	Vertical profile of ozone trends over northern and southern mid-latitudes estimated from ozonesondes, Umkehr, SAGE I, SAGE II, and SBUV(2) for the period 1979–2004.	395
6.7	Ozone anomalies after subtraction of annual cycle, QBO, and solar cycle effects at altitude range from 30 to 40 km	397
6.8	Ozone variations for 60°S–60°N estimated from ground-based data and individual components that comprise ozone variations; and deseasonalized area-weighted total ozone deviations estimated from ground-based data adjusted for solar, volcanic, and QBO effects, for 60°S–60°N	402
6.9	Mean seasonal variations of monthly TOC averaged over the NWR, SWR, WS, ES, FE, and Transcaucasus and Central Asia regions over the period 1973–2002	404
6.10	Propagation paths of ozone anomalies to Europe.	409
6.11	Vertical profile of ozone trends over northern mid-latitudes estimated from ozonesonde, Umkehr, and SBUV(2) measurements for the period 1979–2008	412
6.12	Monthly ozone anomalies for Europe as measured by ozonesondes, SBUV(2), and Umkehr at three pressure layers.	414
6.13	Differences in the ozone and temperature vertical profiles from 2001 (cold stratosphere, low ozone) to 2002 (warm stratosphere, high ozone)	416
6.14	Southern hemisphere total ozone content during September 21–27, 2002 obtained from EP/TOMS observations	417
6.15	Time series of effective temperature for winters 2003–2007 from ECMWF and daily muon rate.	418
6.16	Temperature profiles observed on February 16, 2001 during a major SSW event as well as data from before and after the event over Lerwick, Scotland	420
6.17	Arrhenius plots for temperature-dependent diffusion coefficients for various species in ice as obtained by the LRD depth-profiling technique	422
6.18	Relationship between the factor D_0 of the diffusion coefficient and the activation energy E	423

6.19	Maximum day area covered by the ozone hole, lowest total column ozone, and ozone mass deficiency	426
6.20	O ₃ MD from pre-1976 averages integrated for 105 days (September 1–December 15) for the southern polar region and middle latitudes in the period 1979–2006	428
6.21	Long-term variation of ozone amount at Syowa	430
6.22	Size of the 2007 Antarctic ozone hole compared with the average size for the previous 12 years.	430
6.23	Average total ozone departures from pre-1976 values for the period 1990–2000	432
6.24	Integrated O ₃ MD for a period of 105 days	433
6.25	Total O ₃ MD north of 35°N (January 1–April 15) and south of 35°S (September 1–December 15)	434
6.26	Integrated ozone loss as a function of V_{PSC} for 1992/1993 to 2007/2008.	436
6.27	Seasonal changes of 10-day averaged TOC of each month at the South Pole, Arrival Heights, Syowa Station, and Macquarie Island averaged over the period between 1993 and 2005	438
6.28	Seasonal change in the deviation of TOC from the polar night mean at the South Pole, Arrival Heights, and Syowa Station in the periods 1980–1992 and 1993–2005.	439
6.29	Geographical location of Antarctic stations and the Arctic station chosen for comparison of satellite EP-TOMS and ground-based measurements of total ozone content in 1996–2005	439
6.30	An artificial time series of events of a geophysical parameter in conventional time and in natural time	444
6.31	The entropy in natural time for various window lengths of 3 to 15 years sliding each time by one year through the whole MDOHA time series	445
6.32	The entropy in natural time under time reversal for various window lengths of 3 to 15 years sliding each time by one year through the whole MDOHA time series	446
6.33	The entropy change in natural time under time reversal for various window lengths of 3 to 15 years sliding each time by one year through the whole time series of MDOHA.	447
6.34	Time series of deseasonalized monthly means and the linear regression lines of TOC and tropopause height for 1984–2002 at Athens deduced from <i>in situ</i> observations	475
6.35	Time series of deseasonalized monthly means and the linear regression lines of tropopause temperature deduced from reanalysis data and TOC for 1984–2002 at Athens	476
6.36	Emissions of ODSs and their substitutes	480
6.37	Stratospheric EESC derived for mid-latitude and polar stratospheric regions relative to peak abundances, plotted as a function of time	482
7.1	Calculated monthly concentration of ozone in the surface layer for June 1850	494
7.2	Calculated monthly concentration of ozone in the upper troposphere for June 1850.	494
7.3	Calculated change in annual mean tropospheric ozone in Dobson units between 1850 and 1990.	495
7.4	RF due to the change in tropospheric ozone since pre-industrial times according to the chemistry–transport model	513
7.5	As Figure 7.4, but for the OsloRad model.	514
7.6	Meridional and seasonal distribution of the change in surface air temperature,	

	STL temperature, and STH temperature resulting from STL ozone reduction of 50%	518
7.7	Meridional and seasonal distribution of the adjusted change in net radiation at the tropopause; initial change in short-wave radiative divergence in the STL; and adjusted change in long-wave radiation at the tropopause	519
7.8	Meridional distribution of the change in annual mean surface air temperature for the various scenarios	520
7.9	Meridional distribution of the change in annual mean short-wave, long-wave, and net radiation at the tropopause for the various scenarios	521
7.10	Meridional and seasonal distribution of the change in STL temperature for the TOT(z) scenario and the TOT(φ, z, t) scenario.	522
7.11	Trends in December to February zonal mean zonal wind	543
7.12	Stretched-out and cowboy solutions of the double spherical pendulum problem	552

Tables

1.1	Results of intercomparison of Dobson instruments (July 22 to August 10, 1990) at Arosa, Switzerland	13
1.2	Δ_{ETC} , the error in determination of the extraterrestrial constant for various stray light error models	27
1.3	The results from some stray light experiments taken by the Dobson D118 instrument in Athens between 1992 and 1994.	32
1.4	Layers used for Umkehr ozone profile retrievals	53
1.5	An approximate correction for the air pump temperature	64
2.1	Instruments on board the PRIRODA module of the Mir Space Station.	86
2.2	TOMS main characteristics	89
2.3	General description of OMI	91
2.4	Satellite instrumentation for BUV ozone observations	95
2.5	SBUV/2 wavelengths	96
2.6	TOC trends for January 1979 to March 1995 for five regions of northern mid-latitudes, the Arctic, and Antarctica	103
2.7	Explanation of acronyms for ozone-monitoring instruments found on ozone-monitoring satellites	131
2.8	Chronological summary of ozone-monitoring satellites (or Space Shuttle missions)	134
2.9	Inventory of the most “reliable” datasets with time records longer than 5 years of Ozone Vertical Profile	140
3.1	NDACC and WOUDC ground-based stations contributing to MIPAS O ₃ validation	166
3.2	Results of the comparison between MIPAS v4.61 ozone profiles and NDACC ground-based measurements	175
3.3	Statistical means (MRD) and standard deviations (SD) of the relative differences (X-FTIR)/mean (FTIR) in percent of the O ₃ partial columns defined by the given pressure limits.	182
3.4	Results of the comparison of MIPAS data with mid-latitude ozone soundings	190
3.5	Summary of the coincidences between MIPAS-ENVISAT and MIPAS-B2	192

3.6	Best spatiotemporal coincidences selected for MIPAS-ENVISAT ozone validation with M-55 <i>Geophysica</i> aircraft measurements	203
3.7	Statistics over all comparisons of MIPAS to SAGE II	212
3.8	Statistics over all comparisons of MIPAS to HALOE.	228
3.9	Overview of lidar sites used by Van Gijsel <i>et al.</i> (2009).	233
4.1	The characteristics of total ozone anomalies in January in the equatorial region during negative Southern Oscillation Index anomalies	261
4.2	SBUV(/2) trends in %/decade by seasons and latitudinal zone over the period from January 1979 to May 1994.	264
4.3	Short-term Dobson trends in %/decade using data from January 1979 to February 1994.	265
4.4	Long-term Dobson trends in %/decade using data from January 1964 to February 1994.	265
4.5	Representative TOC trends in %/decade	267
4.6	Long-term total ozone trends derived from ground-based data	292
4.7	Important reactions for odd oxygen balance	302
4.8	Species in photochemical models	304
4.9	Multifractal DFA exponents for reconstructed TOC data at Arosa and Poluy	316
4.10	Calculated percentage change of surface ozone (at four stations) throughout the eclipse event of March 29, 2006 at Athens, Greece	325
4.11	Sites used for detection of the relationship between TOC and tropopause properties.	330
5.1	Chronology of events leading up to the Montreal Protocol	345
5.2	Values of TOC (DU) from Spitsbergen and Halley in 1956 and Halley in 1996	357
5.3	Ratification of the Montreal Protocol	372
5.4	Halons used in various applications	373
5.5	Substances originally included in the Montreal Protocol	374
6.1	Scientific assessment reports	380
6.2	Lifetimes, relative fractional halogen release factors, and ozone depletion potentials for halocarbons	384
6.3a	Comparison of annual changes in stratospheric column ozone and total ozone content in India before and after the implementation of the Montreal Protocol	398
6.3b	Comparison of annual changes in total ozone content in different Indian latitude belts before and after the implementation of the Montreal Protocol	398
6.4	Linear trends at Belsk in selected Umkehr layers and corresponding TOC for the periods 1980–1995 and 1996–2007	399
6.5	Trend results for TOC computed by Yang <i>et al.</i> (2009) for 45°N, 45°S, and integrated 50°N–50°S.	400
6.6	Total ozone linear trends and their deviation from zero significance for periods I, 1973–1992 and II, 1993–2005	405
6.7	Warming and cooling at different heights in some SSWs.	420
6.8	Summary of rate parameters for the diffusion coefficients of selected compounds in ice	422
6.9	Number of days when the Antarctic ozone hole area covered a sunlit surface greater than 10, 15, 20, and 25 km ² from 1995 to 2006	427
6.10	Linear trend from 1987 to 2007 springtime periods in each Umkehr layer at the Japanese Antarctic research station at Syowa.	429
6.11	Geographical co-ordinates of the high-latitude Dobson stations considered by Kravchenko <i>et al.</i> (2009)	440

6.12	Thirteen chemistry–climate models (CCMs)	460
7.1	Gaseous phase chemical reactions included in the model.	488
7.2	Aqueous phase chemical reactions included in the model	490
7.3	Net chemical production of ozone in the planetary boundary layer and the upper troposphere and net upward flux of ozone from the PBL	496
7.4	Radiative forcing due to changes in ozone content for the period 1972–1990	499
7.5	The relative roles of contributions of ozone and other greenhouse gases to the formation of RF	500
7.6	Decadal stratospheric column ozone change, stratospheric ozone forcing, and stratospheric RF gradient for standard tropical profiles	501
7.7	Same as Table 7.6, except for the mid-latitudes	502
7.8	Atmospheric composition changes	503
7.9	SAT and TOC changes	504
7.10	Minor gas concentrations used in RF calculations	505
7.11	Global and annual RF.	505
7.12	Adjusted annual global average net RF from various ozone changes and greenhouse gas changes over different time periods.	507
7.13	January and July clear-sky and average cloudiness sensitivities of ozone and sulfate aerosol and consequent RF for the industrial period 1850–1990	509
7.14	Emission rates applied in the model study of Berntsen <i>et al.</i> (1997)	512
7.15	Simulated global budget of tropospheric ozone	523
7.16	Changes in NO _x emissions due to a 20% reduction in the emissions in each region and the calculated changes in lifetime and steady-state concentration of methane	524
7.17	Total RF due to ozone changes for different regions	525
7.18	Results from perturbing the climate according to paleoclimate data	529
7.19	Results from perturbing the climate according to projected greenhouse gas emission data	530
7.20	Climate impacts of 20% reduction in NO _x	539
7.21	Long-wave, short-wave, and net RF due to stratospheric ozone; global, Northern Hemispheric, and Southern Hemispheric averages, for the four seasons and the yearly average	540

Abbreviations and acronyms

AAO	Antarctic Oscillation
AAOE	Airborne Antarctic Ozone Experiment
AASE 1	Airborne Arctic Stratosphere Expedition
ABL	Atmospheric Boundary Layer
AC&C	Atmospheric Chemistry & Climate
ACCENT	Atmospheric Composition Change: the European Network of Excellence
ACD	Apparent Column Density
ACE	Aerosol Characterization Experiment
ACE-FTS	ACE Fourier Transform Spectrometer
ACVT	Atmospheric Chemistry Validation Team
AD	A and D wavelengths
ADEOS	ADvanced Earth Observing Satellite
AEM-2	Applications Explorer Mission-2
AEMET	Agencia Estatal de METeorología
AES	Atmospheric Environment Service
AF	Adjusted Forcing
AGCM	Atmospheric General Circulation Model
AIRS	Atmospheric InfraRed Sounder
ALA	Aerosol Limb Absorption
ALOMAR	Arctic Lidar Observatory for Middle Atmosphere Research
AM2	Atmosphere Model-2
AMAS	Advanced Millimeter-wave Atmosphere Sounder
AMF	AirMass Factor
AMSR	Advanced Microwave Scanning Radiometer
AMSU	Advanced Microwave Sounding Unit

AO	Arctic Oscillation
AOS	Acousto-Optical Spectrometer
APE	Airborne Polar Experiment
API	Advanced Pollution Instruments
AR	Assessment Report
ARC	ARctic
ARCAS	All-purpose Rocket for Collecting Atmospheric Soundings
ARGOS	Advanced Remote Gaseous Oxides Sensor
amsl	Above mean sea level
ASOPOS	ASsessment of Operating Procedures for Ozone Sondes
ASSET	ASSimilation of EnvisaT data
ASUR	Airborne SUBmillimeter Receiver
ATLAS	ATmospheric Laboratory for Applications and Science
ATMOS	Atmospheric Trace MOlecule Spectroscopy
ATMS	Advanced Technology Microwave Sounder
ATOVS	Advanced TOVS
AURAMS	A Unified Regional Air quality Modeling System
AVE	Aura Validation Experiment
AWI	Alfred Wegener Institut
BADC	British Atmospheric Data Centre
BAPoMON	Background Air Pollution MONitoring Network
BAS	British Antarctic Survey
BASCOE	Belgian Assimilation System for Chemical ObsErvations
BD	Brewer–Dobson circulation
BESOS	Balloon Experiment on Standards for Ozone Sondes
BIC	Balloon Intercomparison Campaign
BIRA	Belgisch Instituut voor Ruimte-Aëronomie
BLISS	Balloonborne Laser In-Situ Sensor
BM	Brewer–Mast (ozonesonde)
BMLS	Balloon Microwave Limb Sounder
BOMEM	BOMEM model FTIR
BP	Band Pass
BSMILES	Balloon-borne Superconducting subMillimeter-wave Limb Emission Sondes
BUV	Backscattered UltraViolet
CALIPSO	Cloud–Aerosol Lidar and Infrared Pathfinder Satellite Observations
Caltech	California Institute of Technology
CAM	Community Atmosphere Model
CANDAC	CANadian Network for the Detection of Atmospheric Change
CAO	Central Aerological Observatory

CARIBIC	Civil Aircraft for the Regular Investigation of the atmosphere Based on an Instrument Container
CC	Cross Correlation
CCD	Convective Cloud Differential; Charge Coupled Device
CCM	Chemistry–Climate Model
CCMVal	Chemistry–Climate Model Validation activity
CCO3L	Coordination Committee on Ozone Layer
CCOL	Coordinating Committee on the Ozone Layer
CCSM	Community Climate System Model
CCSR/NIES	Center for Climate System Research/National Institute for Environmental Studies
CDOM	Colored Dissolved Organic Matter
CEOS	Committee on Earth Observation Satellites
CERES	Clouds and the Earth Radiant Energy System
CF	Cloud cover Fraction
CFC	Chlorofluorocarbon
CFL	Courant–Friedrichs–Levy
CGE	Centro de Geofísica de Évora
CHEM	CHEMistry model
CHEOPS	CHEmistry of Ozone in the Polar Stratosphere
CHRONOS	Canadian Hemispheric and Regional Ozone and Nitrous Oxide System
CHMI	Czech HydroMeteorological Institute
CIRRIS	Cryogenic InfraRed Radiance Instrument for Shuttle
CLAES	Cryogenic Limb Array Etalon Spectrometer
CMAM	Canadian Middle Atmosphere Model
CMDL	Climate Monitoring and Diagnostics Laboratory
CMIP5	Coupled Model Intercomparison Project Phase 5
CNR	Italian National Research Council
CNRS	Centre National de la Recherche Scientifique
CONTRAIL	Comprehensive Observation Network for TRace Gases by AIrLiner
COP-7	Conference of Parties to the Vienna Convention
COPEs	Core Project
CPV	CircumPolar Vortex
CrIS	Cross-track Infrared Sounder
CRISTA	CRyogenic Infrared Spectrometers and Telescopes for the Atmosphere
CTM	Chemistry–Transport Model; Chemical Tracer Model
CTMK	Continuous Time MarKov chain model
CUE	Critical Use Exemption
CUSUM	CUMulative SUM
CWT	Continuous Wavelet Transform
DAAC	Distributed Active Archive Center
DAO	Data Assimilation Office